Letter

pISSN 1225-6161 • eISSN 2287-9307
Korean Journal of Remote Sensing 2025, 41(6), 1269-1274
https://doi.org/10.7780/kjrs.2025.41.6.24

Korean Journal of Remote Sensing
KJRS

Serpentinization Mapping Using Drone Hyperspectral Data

Young-Sun Son*

Senior Researcher, Mineral Exploration and Mining Research Center, Korea Institute of Geoscience and Mineral Resources, Daejeon, Republic of Korea

Abstract: Recent advances in drone hyperspectral technology have led to increased research in the geological community, such as resource exploration and mineral mapping. The dark mineral assemblages found in ultramafic rocks can pose challenges for spectral analysis using drone hyperspectral imagery. This study used the Serpentine Mine as a test site to test drone-based hyperspectral technology for mapping serpentinization in ultramafic rocks. Hyperspectral data were collected using a hyperspectral camera with 490 spectral channels in the wavelength range of 400–2,500 nm. The minimum wavelength mapper technique demonstrated that the drone hyperspectral system can be effectively used to identify serpentinization associated with absorption features occurring at 2,325 nm. Field observations and spectroscopic measurements of rock samples supported the performance of hyperspectral imaging for serpentinization detection. However, reduced sunlight due to cloud cover weakened the absorption characteristics of serpentinization.

Keywords: Drone hyperspectral, Serpentinization, Minimum wavelength mapper, Short-wave infrared

Received: December 6, 2025
Revised: December 11, 2025
Accepted: December 12, 2025
Published: December 31, 2025

Corresponding author:
Young-Sun Son
E-mail: sys6564@kigam.re.kr

1. Introduction

Recent technological advancements in drone platforms and hyperspectral sensors have led to their increasing application in various fields such as geological resources, agriculture, and environmental pollution (Thiele et al, 2021; He et al., 2022; Lee et al., 2024). A hyperspectral sensor records the reflectance or emissivity of objects in the form of images. When electromagnetic radiation is incident on the surface of a mineral or rock, some wavelengths of light are absorbed by the mineral particles, while other wavelengths are reflected. Reflectance is the ratio of the intensity of the incident light to the intensity of the light reflected from the object, and a mineral exhibits a unique spectrum depending on its physical and chemical properties. In the visible/near infrared (VNIR) wavelength range (400–1,100 nm), absorption occurs due to transition metals (e.g., Fe^{2+}, Fe^{3+}, Mn, Ti) that absorb light at wavelengths necessary to excite electrons. In the short-wave infrared (SWIR) wavelength range (1,100–2,500 nm), vibrational processes caused by subtle movements of molecules or bonded nuclei due to incident radiation create unique absorption characteristics of minerals. In particular, H_2O, OH, and CO_3 contained in clay minerals, sulfate minerals or carbonate minerals cause absorption at specific wavelengths, which enables mineral identification (Clark et al., 2003).

Nickel is a silvery metal element mainly used to make stainless steel and alloys able to withstand extreme temperatures and corrosive environments. Today, more than 70% of global production is used to make stainless steel; however, demand for the compound is increasing as it is an essential component of electric vehicle batteries. Nickel mineralization associated with serpentinization primarily occurs when ultramafic rocks undergo metamorphism and hydrothermal processes to transform into serpentine, resulting in nickel accumulation. Nickel has also been reported in ultramafic rocks in Andong, South Korea (Davaasuren et al., 2024). The Andong ultramafic body is located on the northern border of the Gyeongsang Basin and is oval-shaped, measuring 3.5 × 1.2 km^2. This body has undergone serpentinization of varying intensity and includes the Andong open-pit serpentinite mine.

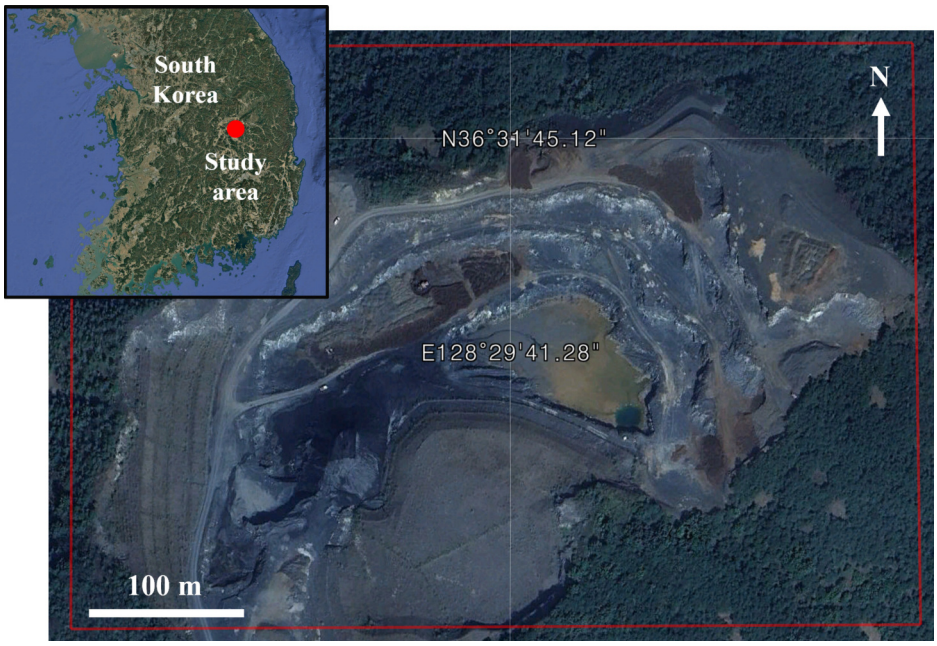

Fig. 1. Google Earth images showing the location of the Andong serpentine mine in Korea and the drone hyperspectral imaging area (red box).

The goal of this study was to evaluate the utility of drone hyperspectral imaging for identifying ultramafic rocks with serpentinization at a serpentine mine in Andong, South Korea (Fig. 1). In this study, we map serpentinization based on the spectral absorption wavelength positions and depths of VNIR-SWIR hyperspectral data collected by a drone. To validate the effectiveness of this Imaging spectroscopy technique, rock samples were collected from outcrops of serpentinite and ultramafic rocks. A serpentine map can aid in monitoring mine development and asbestos-related environmental contamination.

2. Materials and Methods

2.1. Data Acquisition and Preprocessing

Hyperspectral data was collected using the HySpex Mjolnir VS-620 system mounted on a Gremsy gStabi H16 XL gimbal fixed to a BFD 1400 SE8 drone. The system can simultaneously acquire hyperspectral data with up to 1,024 spatial pixels in the VNIR (400–1,000 nm) and 620 spatial pixels in the SWIR (970–2,500 nm). Between 1:00 PM and 3:00 PM, on October 16, 2024, we collected hyperspectral data from five flight lines at an altitude of 200 m and a flight speed of 4 m/s. The swath of each line was approximately 50 m. The frame times were set to 13.5 (VNIR) ms and 27 ms (SWIR), respectively, and the integration times were set to 13 ms (VNIR) and 26.8 ms (SWIR). These settings resulted in spatial resolutions of 5.4 cm and 10.8 cm for the VNIR and SWIR images, respectively.

Radiometric calibration was performed on the VNIR and SWIR raw data using HySpex RAD software provided by the sensor manufacturer. This process converts digital numbers into radiance values at the sensor and corrects for optical distortions (keystone and smile effects) caused by spatial and spectral misregistration of each pixel (Nieke et al., 2008). Changes in sensor position and orientation due to drone shaking during flight cause geometric distortion. The accurate position and orientation information recorded in the Applanix APX-20 inertial processing unit mounted on the Hyspex Mjolnir sensor system was used to model and remove the geometric distortion using Applanix POSPAC and HySpex NAV programs (Son, 2024).

At-sensor radiance data are influenced by the solar irradiance spectrum and atmospheric effects, including absorption (particularly by water vapor, O_2, and CO_2) and scattering by particles and gases (Green et al., 1988). To remove these effects and convert the radiance data to reflectance, we used drone atmospheric correction (DROACOR) software, developed based on radiative transfer modeling that considers the characteristics of drone hyperspectral data. Atmospheric correction using a radiative transfer model requires detailed information such as data acquisition time, location (latitude/longitude), solar angle, observation angle, sensor internal geometry, terrain height, and sensor altitude. DROACOR retrieves additional parameters for atmospheric correction, such as water vapor content and aerosol optical depth, from the image

 https://doi.org/10.7780/kjrs.2025.41.6.24

average using a spectral fitting technique at 550 nm (Thompson et al., 2018). Based on a digital surface model, terrain-induced irradiance variations and shadows were corrected, and bidirectional reflectance distribution function (BRDF) effects due to observation angle were also corrected.

2.2. Minimum Wavelength Mapping and Collection of Rock Sample Spectra

We analyzed the spectral characteristics associated with serpentinization using the minimum wavelength mapper (MWM). MWM provides information on the dominant mineral per pixel by mapping the wavelength locations of the deepest absorption features in a spectroscopic image (Hecker et al., 2019). First, we define the wavelength range where the absorption features appear and perform continuum removal by dividing the convex hull over this wavelength range. We then model the continuum-removed reflectance using only three data points centered around the maximum absorption point. This allows us to define a quadratic equation with three unknowns, which can be directly substituted into the equation to obtain the wavelengths as follows (Rodger et al., 2012):

$$\rho_{cr} = a\lambda^2 + b\lambda + c \quad (1)$$

where, ρ_{cr} is the continuum-removed reflectance at wavelength λ, and a, b, and c are fitting coefficients.

$$\omega_{min} = -\frac{b}{2a} \quad (2)$$

where, ω_{min} is the interpolated wavelength position at minimum reflectance, and a and b are the coefficients of the parabola function.

Finally, the depth of the deepest absorption feature of the interpolated continuum-removed reflectance is calculated as follows:

$$D_{cr} = 1 - (a\lambda_{true}^2 + b\lambda_{true} + c) \quad (3)$$

To validate the detection of serpentinization characteristics from drone hyperspectral imagery, spectral measurements were performed on surface rock samples (six locations) using a portable spectrometer. Spectra were acquired from two to four locations for each rock sample.

3. Results and Discussion

Fig. 2 shows the reflectance spectrum of serpentine from the U.S. Geological Survey (USGS) spectral library. Serpentine exhibits strong absorption at 2,325 nm and 2,335 nm. Serpentine samples collected from our study area similarly exhibited strong absorption between 2,320 and 2,335 nm (blue spectra in Fig. 3). Furthermore, the wavelength locations of the maximum absorption features in the drone hyperspectral spectra from the locations where these rock samples were collected were also mostly between 2,320

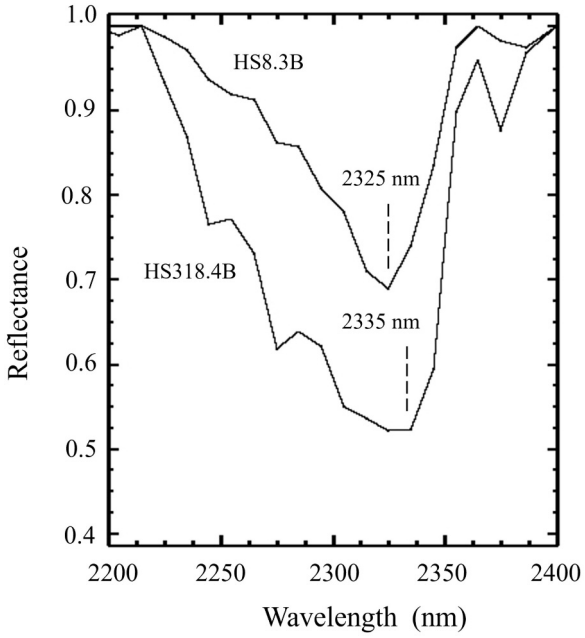

Fig. 2. Continuum-removed reflectance spectra of serpentine in the USGS library (Clark et al., 2007).

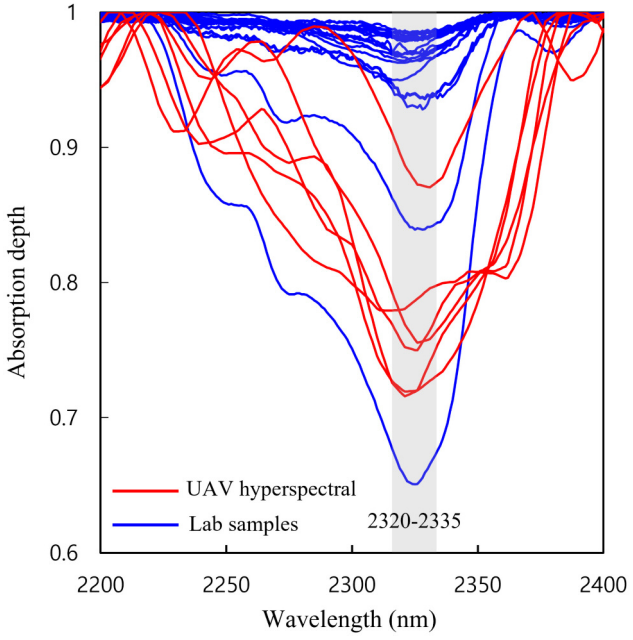

Fig. 3. Comparison between drone hyperspectral and laboratory spectra with continuum removal.

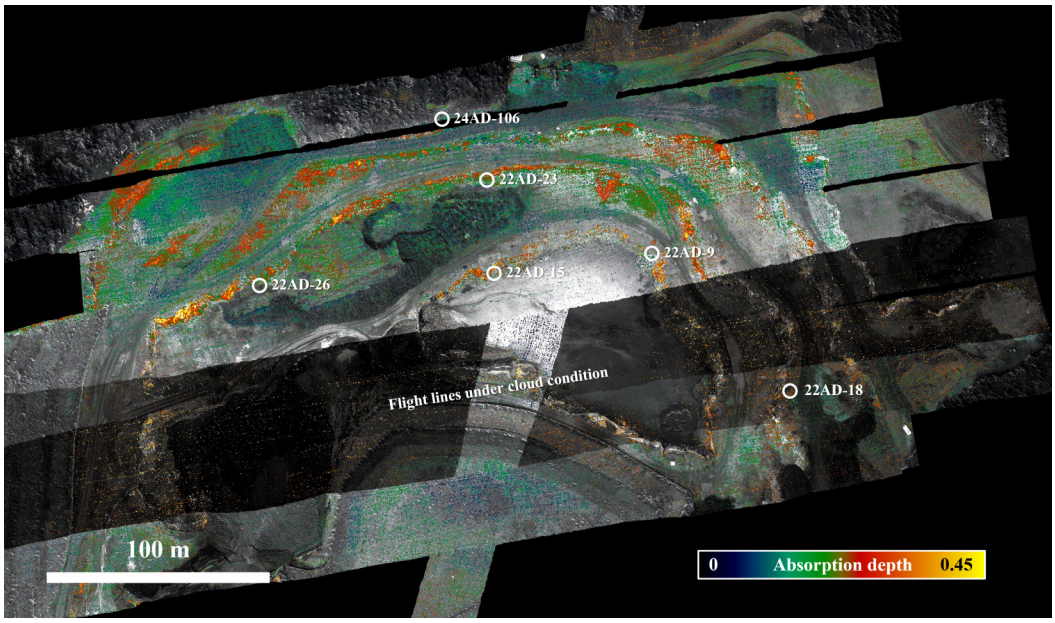

Fig. 4. Minimum wavelength showing the distribution of serpentinization in the Andong deposit. The white circles indicate rock sampling locations and sample numbers.

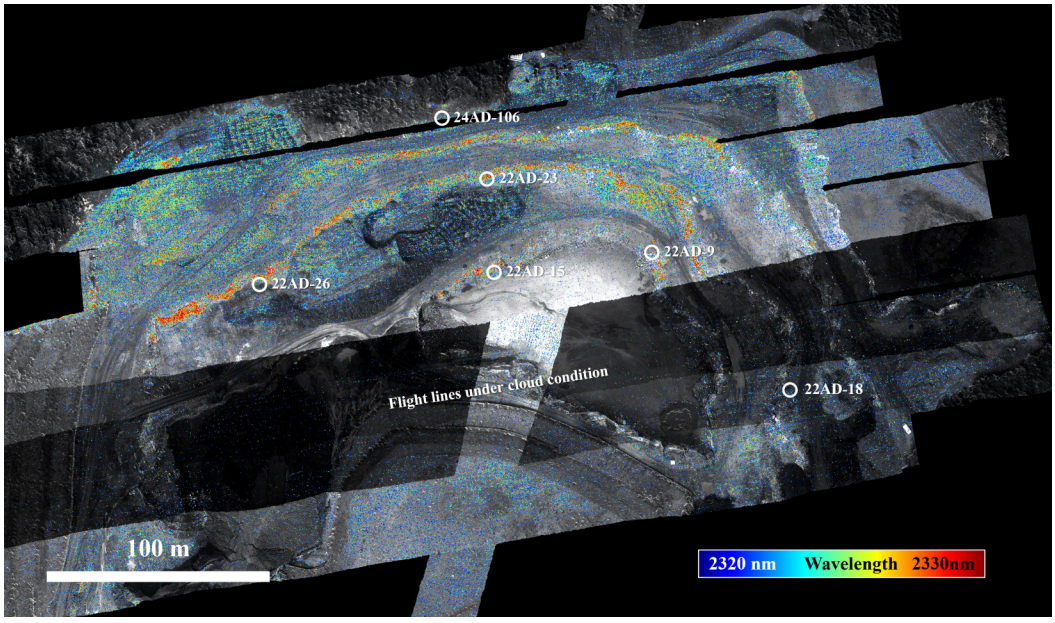

Fig. 5. Absorption depth map showing the distribution of serpentinization in the Andong deposit. The white circles indicate rock sampling locations and sample numbers.

and 2,335 nm (red spectra in Fig. 3). These absorption features were used to map the compositional distribution of serpentine throughout the mine, allowing the identification of serpentine along the open pit mine benches (Fig. 4). The absorption maximum in these areas was found to occur at relatively long wavelengths (near 2,330 nm).

A visualization generated using absorption depth (Fig. 5) highlights differences in absorption intensity, suggesting stronger serpentinization or more abundant serpentine. The strong absorption also occurs primarily along the open-pit benches. In contrast, hyperspectral flight line images taken under cloud-obscured conditions revealed a weakening of absorption intensity due to serpentinization within the ultramafic rock. This is likely to have a greater impact on the signal-to-noise ratio, particularly

 https://doi.org/10.7780/kjrs.2025.41.6.24

in ultramafic rocks where the dark rock color results in a weaker spectral reflectance.

The results of this study demonstrate the performance of a drone-based hyperspectral camera in identifying the distribution of serpentine in open-pit mines. The serpentinization areas extracted from the drone hyperspectral data were verified through field investigations and mineralogical and chemical analyses of rock samples. Caution is required when using the MWM technique, as the absorption wavelengths of serpentine are similar to those of some minerals, such as calcite, dolomite, and chlorite.

Other characteristics, such as the shape of the spectrum and the symmetry of the absorption depth, may be considered to differentiate them. Previous studies have shown that the intensity of absorption features in alteration minerals is closely related to mineral abundance. However, this is also influenced by particle size, sorting, and porosity. The number of samples in this study was insufficient to quantitatively link hyperspectral absorption depth to the degree of serpentinization. Further research with a larger sample size is needed. Serpentinization mapping using a drone-based hyperspectral approach can aid mine operations by providing aerial views of the distribution of serpentine, which is difficult to detect using ground sensors or field surveys. Furthermore, it is expected to be useful in assessing asbestos-related geohazards.

4. Conclusions

This study evaluated the utility of drone hyperspectral imaging for identifying ultramafic rocks with serpentinization in a serpentine mine. Using the MWV technique, serpentinization was mapped based on spectral absorption wavelength locations and depths in the SWIR. This study did not consider the effects of mineral mixing within mafic rocks. Future work plans include evaluating the impact of various mineral mixing on the absorption properties of serpentine and investigating its relevance to mineralization for nickel exploration.

Author Contributions

Conceptualization, Data curation, Formal analysis, Investigation, Methodology, Validation, Writing–original draft, Writing–review & editing: Son YS.

Conflicts of Interest

No potential conflict of interest relevant to this article was reported.

Funding

This work was supported by the Korea Institute of Geoscience and Mineral Resources (KIGAM) Basic Research Project (25-3212) funded by the Ministry of Science and ICT of Korea.

Data Availability Statement

The data that support the findings of this study are available from the corresponding author upon reasonable request.

Acknowledgments

None.

Supplementary Materials

None.

References

Clark, R. N., Swayze, G. A., Livo, K. E., Kokaly, R. F., Sutley, S. J., Dalton, J. B., et al., 2003. Imaging spectroscopy: Earth and planetary remote sensing with the USGS Tetracorder and expert systems. *Journal of Geophysical Research: Planets, 108*(E12), 5131. https://doi.org/10.1029/2002JE001847

Clark, R. N., Swaze, G. A., Wise, R. A., Livo, K. E., Hoefen, T. M., Kokaly, R. F., et al., S.J., 2007. *USGS Digital Spectral Library Splib06a* (Data Series 231). U.S. Geological Survey. https://doi.org/10.3133/ds231

Davaasuren, O.-E., Koh, S.-M., Lee, B. H., and Heo, C.-H., 2024. Serpentinization and potential Ni-Cr mineralization of the Andong ultramafic block in South Korea. *Resource Geology, 74*(1), e12331. https://doi.org/10.1111/rge.12331

Green, A. A., Berman, M., Switzer, P., and Craig, M. D., 1988. A transformation for ordering multispectral data in terms of image quality with implications for noise removal. *IEEE Transactions on Geoscience and Remote Sensing, 26*(1), 65–74. https://doi.org/10.1109/36.3001

He, J., DuPlessis, L., and Barton, I., 2022. Heap leach pad mapping with drone-based hyperspectral remote sensing at the Safford Copper Mine, Arizona. *Hydrometallurgy, 211*, 105872. https://doi.org/10.1016/j.hydromet.2022.105872

Hecker, C., van Ruitenbeek, F. J. A., van der Werff, H. M. A., Bakker, W. H., Hewson, R. D., and van der Meer, F. D.,

2019. Spectral absorption feature analysis for finding ore: A tutorial on using the method in geological remote sensing. *IEEE Geoscience and Remote Sensing Magazine, 7*(2), 51–71. https://doi.org/10.1109/MGRS.2019.2899193

Lee, I., Kim, H.-M., Kim, Y., Ahn, H., Ryu, J.-H., Jeong, H., et al., 2024. Spatiotemporal monitoring of soybean growth and water status using drone-based shortwave infrared (SWIR) imagery. *Korean Journal of Remote Sensing, 40*(3), 275–284. https://doi.org/10.7780/kjrs.2024.40.3.4

Nieke, J., Schlapfer, D., Dell'Endice, F., Brazile, J., and Itten, K. I., 2008. Uniformity of imaging spectrometry data products. *IEEE Transactions on Geoscience and Remote Sensing, 46*(10), 3326–3336. https://doi.org/10.1109/TGRS.2008.918764

Rodger, A., Laukamp, C., Haest, M., and Cudahy, T., 2012. A simple quadratic method of absorption feature wavelength estimation in continuum removed spectra. *Remote Sensing of Environment, 118*, 273–283. https://doi.org/10.1016/j.rse.2011.11.025

Son, Y.-S., 2024. Evaluation of the DROACOR model for atmospheric correction of drone hyperspectral data. *Korean Journal of Remote Sensing, 40*(6), 1275–1281. https://doi.org/10.7780/kjrs.2024.40.6.1.31

Thiele, S. T., Lorenz, S., Kirsch, M., Cecilia Contreras Acosta, I., Tusa, L., Herrmann, E., et al., 2021. Multi-scale, multi-sensor data integration for automated 3-D geological mapping. *Ore Geology Reviews, 136*, 104252, https://doi.org/10.1016/j.oregeorev.2021.104252

Thompson, D. R., Guanter, L., Berk, A., Gao, B.-C., Richter, R., Schläpfer, D., et al., 2018. Retrieval of atmospheric parameters and surface reflectance from visible and shortwave infrared imaging spectroscopy data. *Surveys in Geophysics, 40*, 333–360. https://doi.org/10.1007/s10712-018-9488-9